

## Polyethylene oxide matrix tablet swelling evolution: The impact of molecular mass and tablet composition

PETRA DRAKSLER<sup>1,3,\*</sup>  
URŠA MIKAC<sup>2</sup>  
PETER LAGGNER<sup>4</sup>  
AMRIT PAUDEL<sup>4,5</sup>  
BILJANA JANKOVIĆ<sup>1,3,\*</sup>

<sup>1</sup> Department of Pharmaceutical Technology  
Faculty of Pharmacy, University of  
Ljubljana, 1000 Ljubljana, Slovenia

<sup>2</sup> Jožef Štefan Institute, 1000 Ljubljana  
Slovenia

<sup>3</sup> Sandoz Development Center, Lek d.d.  
1526 Ljubljana, Slovenia

<sup>4</sup> Research Center for Pharmaceutical  
Engineering (RCPE) GmbH, 8010, Graz  
Austria

<sup>5</sup> Institute of Process and Particle  
Engineering, Graz University of Technology  
8010, Graz, Austria

This article describes the designing of matrix tablets composed of polyethylene oxides (PEOs) with relative molecular masses of  $1 \times 10^6$ ,  $2 \times 10^6$ , and  $4 \times 10^6$ . Percolation thresholds were determined for all of the selected PEO formulations (18, 16, and 12 %, *m/m*), taking into consideration excipients and tablet surface area which significantly increased the percolation threshold. Moreover, the robustness of the gel layer in PEO matrix tablets was evaluated by magnetic resonance imaging under various mechanical stresses (no flow,  $12 \text{ mL min}^{-1}$ , and  $64 \text{ mL}^{-1}$  of medium flow). Correlations between the percolation threshold and gel thickness ( $R^2 = 0.86$ ), gel thickness and the erosion coefficient ( $R^2 = 0.96$ ) was detected. Furthermore, small-angle X-ray scattering of the selected PEOs detected differences in polymer molecular complexity at the nanoscale. Finally, the ratio of the heat of coalescence to the heat of fusion has confirmed the PEO molecular mass-dependent percolation threshold.

**Keywords:** polyethylene oxide, MRL, percolation threshold, SAXS, WAXS

Accepted June 6, 2020

Published online June 16, 2020

Hydrophilic matrix tablets are the most commonly used drug delivery systems for extended drug release with zero-order release kinetics, which sustain constant *in vivo* plasma concentrations. High relative molecular mass ( $M_r$ ) polyethylene oxides (PEOs) are non-toxic, non-ionic, water-soluble polymers used in the development of controlled delivery systems (1–3). Due to their hydrophilic character, PEOs swell upon contact with body fluids. During hydration, a gel layer is formed around the tablet core, generating a fluid diffusion barrier and simultaneously restricting drug diffusion into the medium. With increasing polymer  $M_r$ , a thicker and more robust gel is formed, resulting in a slower dissolution and higher resistance of the gel layer to mechanical stresses (1, 2). The polymer swelling rate depends on molecular characteristics (chain length, the radius of gyration, contour length, and end-to-end distance), which define the elastic properties of polymers

\* Correspondence; e-mail address: biljana.jankovic@ffa.uni-lj.si; biljana.jankovic@sandoz.com,  
petra.draksler@sandoz.com

and consequently their swelling rate (4). The PEO polymer swelling properties also depend on the number and types of interactions in an aqueous environment that determine the connections between polymer chains and therefore viscosity, swelling, and gel formation (5–7). The effect of the morphology of hydrated drug-loaded polymer matrices on erosion, drug release, and degradation is well described (8) and mainly depends on the ratio of hydrophobic and hydrophilic domains in the molecular structure (9, 10). Moreover, the difference in PEO crystallinity is reflected in various lamellar thicknesses, and this generally impacts the burst effect upon drug release (11, 12).

As a state-of-the-art variable, different excipients can change polymer hydration. The literature explains how the hydration of PEG-containing copolymers (13), their structure (14), and the clustering of water in polymers (15) affect drug release and polymer resorption. The disruption of polymer chains is caused by the interactions between water molecules and polymer chains, which can result in phase separation of the polymer domains and a faster drug release. To ensure constant controlled drug release, the gel thickness in hydrophilic matrix systems should be unsusceptible to applied mechanical stresses. This can be attained with polymer concentrations above the percolation threshold (*i.e.*, the concentration that ensures the formation of a uniform and robust gel layer around the tablet core). Percolation threshold concentrations have been extensively studied in hydroxypropyl methylcellulose (HPMC) formulations (16–20), but not for PEOs with  $M_r$  of  $1 \times 10^6$ ,  $2 \times 10^6$ , and  $4 \times 10^6$ . Therefore, for the successful development of matrix tablets with constant drug release, the impact of different excipients on the swelling process should be well understood.

Nuclear magnetic resonance (NMR) and magnetic resonance imaging (MRI) are used as non-invasive approaches for investigating gel formation upon polymer hydration with improved measurement precision (21–24). Moving front positions and polymer concentration in the gel layer during tablet hydration are characterized by  $T_2$ -mapping (25),  $T_1$ -weighted (26, 27), and diffusion-weighted (28) MRI methods. This also allows the simultaneous measurement of the gel formation and the drug release either by a combination of  $^1\text{H}$  and  $^{19}\text{F}$  MRI (29–31) or by using a flow-through cell with a combination of MRI and UV-VIS spectrometry (32).

Only a few studies of MRI applications in research on PEO matrix tablets and effects of composition (27, 28) and mechanical stresses (1, 3, 33) on their gel thickness have been reported separately, without a focus on microstructural polymer characteristics.

The objective of this study is systematic, qualitative, and quantitative determination of molecular differences between selected PEOs with  $M_r$  of  $1 \times 10^6$ ,  $2 \times 10^6$ , and  $4 \times 10^6$ . Wide-angle X-ray scattering (WAXS) and small-angle X-ray scattering (SAXS) were applied to detect the differences in microstructures (polymer molecular dimension, size, structure, crystallinity, and pore sizes) of selected PEO polymers. DSC and hot-stage optical microscopy were used to gain better insight into the polymer structure. To confirm the differences detected at the microscopic level, MRI was used with the addition of detecting moving fronts in the PEO prolonged-release tablets (PRTs). The study also includes the impact of formulation composition as well as the mechanical stress effect on gel formation and drug release. Ultimately, a separate percolation threshold study was performed on selected PEO PRTs using binary and multicomponent systems in order to elucidate how the tablet's shape and composition affect the PEO percolation threshold.

## EXPERIMENTAL

### Materials

Three different  $M_r$  of PEO (Polyox<sup>TM</sup>, Dow-Colorcon, Dartford, UK) were used: low ( $1 \times 10^6$ ), medium ( $2 \times 10^6$ ), and high ( $4 \times 10^6$ ). The model drug with  $M_r$  of 397 Da and low apparent permeability (BCS class III) was used. Its calculated dose/solubility volume is less than 15 mL in aqueous buffer solutions, with a physiological pH range from 1 to 7.5. The model drug structure has four hydrogen bond donors and six hydrogen bond acceptors. All other chemicals and solvents were of analytical grade and were used without further purification. The reagents NaOH,  $\text{KH}_2\text{PO}_4$ , and  $\text{H}_3\text{PO}_4$  used for the dissolution testing and HPLC assay, were purchased from Merck, Germany. Acetonitrile was obtained from J. T. Baker, US. For all experiments, a medium phosphate buffer with a pH of 6.8 was used throughout the study, prepared with deionized water.

### SWAXS analysis of the selected PEOs

The nanostructures and crystallinity of three PEOs were analyzed using simultaneous small- and wide-angle X-ray scattering (SWAXS). SWAXS measurements were performed using an S3-MICRO SWAXS system (Bruker AXS, formerly Hecus X-ray Systems, Austria) featuring a Cu K $\alpha$  X-ray microsource (Xenocs, France) with point-focusing optics. Samples were contained in X-ray capillaries with a 1.5 mm inner diameter and rotated during exposure at  $\approx 0.2$  Hz in a temperature-controlled cuvette (TCCS and SpinCap, Hecus). Exposure times were generally 5 min/sample. Scattering signals were simultane-

*Table I.* PEO test formulations (TF) containing PEOs with different molecular masses, polyethylene glycol (PEG), other excipients and model drug belonging to class III of biopharmaceutical classification system (BCS)

Composition (%)	TF										
	1	2	3	4	5	5b	6	6a	6b	6c	7
Low- $M_r$ PEO	100				27	27					
Intermediate- $M_r$ PEO	100		38.5			27	23	27	35		
High- $M_r$ PEO		100								27	27
PEG			61.5		48		52	48	40	48	48
Other excipients (filler, binder, and water-soluble components)								5			
Model drug (BCS III)							20				
Tablet shape	round		round	oval	round		oval		round	oval	
Tablet surface area (mm <sup>2</sup> )	309		309	196	309		196		309	196	

ously detected in the SAXS ( $0.06\text{--}8^\circ 2\theta$ ) and WAXS ( $17\text{--}27^\circ 2\theta$ ) regions by two linear position-sensitive detectors (Hecus PSD-50). The fractal dimensions (Ds) were derived from the slope in the double-logarithmic SAXS-plots (34). The WAXS profiles were used to obtain information on the relative degree of crystallinity in the semi-crystalline PEO systems based on the Bragg peaks characteristic of PEOs. Furthermore, Micro-DSC analysis of the PEO powders was performed using MicroCalix (Setaram, France). A complementary set of thermal analyses was performed using polarized hot-stage optical microscopy from room temperature to  $200\text{ }^\circ\text{C}$  at a heating rate of  $2\text{ }^\circ\text{C min}^{-1}$ .

#### *Formulation of PEO PRTs*

Test formulations (TF) 1–4 were prepared using manual sieving, mixing, and compression to form round 250 mg tablets with a 12 mm diameter or oval 250 mg tablets (Table I). Moreover, samples of pure PEO polymers were prepared (TF 1–3) and TF of medium- $M_r$  PEO with the addition of PEG with  $M_r$  of 8000 (TF 4) as well as with variation of PEG 8000 addition (TF 6a–c). The coating effect on drug release and swelling properties was evaluated at the beginning of the study.

#### *Preparation of PEO binary systems*

For the percolation threshold study, several binary mixtures of selected PEO polymers and the model drug in different mass concentration ranges were prepared (Table II, TFs X–Z) in order to determine the critical polymer concentration for the formulation of a robust hydrogel. Blends were then compressed into 250 mg round 12 mm tablets. A drug release study was conducted using the dissolution method described in section *Drug release study from PEO PRTs* below using a standard paddle apparatus (Apparatus II, VanKel Dissolution Apparatus, model VK 7000, USA).

#### *Preparation of reference PEO gel samples*

Gels with a polymer mass ratio (*m/m*) ranging from 1 to 100 % of all selected PEOs were prepared using purified water and a potassium phosphate buffer with a pH of 6.8. Various gel preparation approaches were used: *i*) for PEO concentrations between 1 and 30 %, PEO with a selected  $M_r$  was weighed and dispersed in the selected medium with a magnetic stirrer until a uniform gel was formed; *ii*) for gel concentrations between 30 and 50 % polymer, PEO with a selected  $M_r$  was placed in a desiccator with salts of defined relative humidity and equilibrated; *iii*) For PEO concentrations higher than 50 %, a prede-

*Table II. Composition of binary test formulations (TF), containing PEOs with different molecular masses in different ratios*

TF	PEO $M_r$	Polymer concentration range (%)	TF
X	$1 \times 10^6$	10–90	X10–X90
Y	$2 \times 10^6$	10–90	Y10–Y90
Z	$4 \times 10^6$	10–90	Z10–Z90

terminated amount of medium was added to PEO powder with a selected  $M_r$  in the sealed beaker and equilibrated; *iv)* for 100 % PEO samples, PEO powder was dried in a vacuum dryer to absolute dryness at 60 °C.

#### *PEO gels NMR relaxation times*

For gels of known PEO concentration in both media (water and a potassium phosphate buffer with a pH of 6.8), the NMR spin-lattice ( $T_1$ ) and spin-spin ( $T_2$ ) relaxation times were measured at room temperature and at a  $^1\text{H}$  NMR frequency  $\nu_{\text{H}} = 100$  MHz. Tecmag Apollo (Tecmag, USA) an MRI spectrometer with a superconducting 2.35 T horizontal bore magnet (Oxford Instruments, UK) equipped with gradients and RF coils for MR microscopy (Bruker, Germany) was used for the experiments. A standard inversion recovery sequence (35) ( $180^\circ - \tau - 90^\circ - \text{AQ}$ ) by changing  $\tau$  values from 0.02 ms to 15 s was used to measure the  $T_1$  time. The  $T_2$  times of gels with polymer concentrations lower than 80 % were measured using a CPMG pulse sequence (9) ( $90^\circ - \tau - (180^\circ - \tau - \text{AQ} - \tau)_N$ ) with  $\tau = 1$  ms and  $N = 3,000$ . For samples at higher PEO concentrations ( $> 80$  %) with short  $T_2$  ( $T_2 < 5$  ms), the  $T_2$  times were measured by a Hahn echo pulse sequence by changing the inter-echo time from 0.02 ms to 2 s.

#### *MRI of swelling PEO PRTs*

The tablet for MRI was inserted into a container so that only one cylinder base was exposed for the medium penetration. After 10 minutes of tablet swelling the first MR image was taken and then every 30 minutes for 15 hours.

The same spectrometer as used for the relaxation time measurements was used to record the MRIs at room temperature. Two different MRI methods were used in order to determine the erosion, swelling, and penetration front positions upon tablet swelling. To measure the positions of the erosion and swelling fronts, a 2D  $T_1$ -weighted MRI was taken using a standard spin-echo pulse sequence (35) with echo time (TE) of 6.2 ms and repetition time (TR) of 200 ms. The field of view was 50 mm with an in-plane resolution of 200  $\mu\text{m}$  and a slice thickness of 3 mm. A one-dimensional single point imaging (1D SPI) sequence was used to detect the medium penetration into the tablet. A single point on the free induction decay was sampled at encoding time  $t_p = 0.17$  ms after the radiofrequency detection pulse  $\alpha = 20^\circ$  with TR of 200 ms with a resolution of 350  $\mu\text{m}$ .

The MRI experiments were repeated with the flow-through cell in order to determine the gel thickness during swelling and drug release under the same conditions. A container with 900 mL of medium was connected to a homemade MRI flow-through cell using plastic tubes. The medium flow was driven by a peristaltic pump (Anko, USA) and controlled at two different flow rates:  $12 \pm 2$  and  $64 \pm 2$  mL min $^{-1}$ . Because the MR images were acquired during flow, motion artefacts were observed in the area where only the medium was present. On the other hand, no artefacts were observed in the gel because the gel was hard enough so that the flow did not provoke large gel movements. This was confirmed by comparing the two consecutive images, first without flow and immediately thereafter with the flow, and the same gel thicknesses were determined from both images.

The measurements were repeated at least three times for each kind of experimental setting and tablet.

### *Drug release study from PEO PRTs*

Drug release from PEO PRTs was evaluated with a “non-mixing” (static) and “mixing” (dynamic) method during MRI measurements and with the standard paddle method (USP Apparatus 2, with three repetitions  $n$ ). The standard paddle method was performed on a fully calibrated dissolution apparatus (Apparatus II, VanKel Dissolution Apparatus, model VK 7000, USA) with a paddle speed of 50 rpm, temperature  $37 \pm 0.5$  °C, and 900 mL of medium phosphate buffer with a pH of 6.8. At predetermined time intervals, 1.7 mL samples were withdrawn without being replaced.

To study drug release using the “non-mixing” method, tablets were inserted into the same containers as for MRI measurements. Medium penetration was allowed from only one circular surface, with no medium mixing. Ten containers with each type of tablet (Table I) were prepared and 5.2 mL of the medium was added to all containers at the same time. The medium was removed from one of the containers at the same time points as for the paddle method, and drug content was determined as described above. Additionally, drug release was measured with the “mixing” method. Here the medium flow was used at two different flow rates (*i.e.*,  $12 \pm 2$  and  $64 \pm 2$  mL min<sup>-1</sup>) to study the influence of mechanical stress on drug release. The 5 mL samples were withdrawn without being replaced from the 900 mL container at predetermined time intervals.

The collected samples were filtered through a filter with 1.0 µm pores and analyzed using HPLC, with UV detection at a wavelength of 249 nm (Agilent 1100Series Agilent Technologies, Germany). An XTerra column C18 3.5 µm (150 × 4.6 mm; Waters, USA) was used. The mobile phase represented the mixture of phosphate buffer (pH 4.0) and acetonitrile in a 1:3 ratio, respectively. The fraction of drug release  $Q =$  was plotted as the function of time, where  $m_t$  is mass of the drug released at time  $t$  and  $m_\infty$  is mass of the drug that can be released at infinite time, and thus is considered equal to the drug loading in the tablet.

### *Determination of the erosion and diffusion contributions to drug release*

A semi-empirical model developed by Narasimhan and Peppas was used to determine erosion and diffusion contributions to drug release (36). The model considers two moving boundaries: the swelling front  $R$  and the erosion front  $S$ , and it defines the gel layer thickness as  $S-R$ . A steady-state solution to the model equations gives the dependence of the gel layer thickness at time  $t$  as:

$$-\frac{S-R}{B} - \frac{A}{B^2} \ln \left[ 1 - \frac{B}{A}(S-R) \right] = t \quad (1)$$

and the expression for the fraction of the released drug  $Q$  as:

$$\begin{aligned} Q &= \frac{v_{\text{deq}} + v_d^*}{l} \left( \sqrt{2A8t - t_0} + B(t - t_0) \right) \\ &= k_d \sqrt{(t - t_0)} + k_r(t - t_0) \end{aligned} \quad (2)$$

where  $l$  is the tablet thickness, and  $v_{\text{deq}}$  and  $v_1^*$  are the drug equilibrium volume fractions at gel-medium interface  $S$  and at glassy-gel interface  $R$ , respectively. To be able to describe the experimental data, the delay time  $t_0$  was added to Eq. 2. Namely, at higher flow rates, larger pieces of the gel can be removed from the gel layer and the drug cannot be immediately released into the medium because of the large size of the torn pieces. The term  $A$  describes the Fickian diffusion of the drug through the gel layer and is given as:

$$A = D_1(v_{1\text{eq}} - v_1^*) \left( \frac{v_{1\text{eq}}}{v_{1\text{eq}} + v_{\text{deq}}} + \frac{1}{v_1^* + v_{\text{d}}} \right) \\ + D_{\text{d}}(v_1^* - v_{\text{deq}}) \left( \frac{v_{\text{deq}}}{v_{1\text{eq}} + v_{\text{deq}}} + \frac{1}{v_1^* + v_{\text{d}}} \right) \quad (3)$$

The term  $B$  describes chain disentanglement and dissolution leading to Case II transport, in which drug release is controlled by polymer erosion and is given as:

$$B = \frac{k_{\text{dis}}}{v_{1\text{eq}} + v_{\text{deq}}} \quad (4)$$

where  $D_1$  and  $D_{\text{d}}$  are the diffusion coefficients of the medium and drug, respectively.  $v_1^*$  and  $v_{1\text{eq}}$  are the medium equilibrium volume fractions at interface  $S$  and at interface  $R$ , respectively, and  $k_{\text{dis}}$  is the disentanglement rate of the polymer chains, which can be given as the ratio of the radius of gyration  $r_g$  and the reptation time  $t_{\text{rept}}$ ,  $k_{\text{dis}} = r_g/t_{\text{rept}}$ . Eq. 2 can be simplified by defining the diffusion rate constant and the erosion rate constant. The  $k_{\text{d}}$  and  $k_r$  can be used to calculate the diffusion ( $D$ ) and erosion ( $E$ ) contributions to drug release as in the Peppas-Sahlin model, Eq. 5 (37).

$$D = \frac{1}{1 + \frac{k_r}{k_d} \cdot t^{0.5}} \quad (5)$$

and

$$E = 1 - D = \frac{\frac{k_r}{k_d} \cdot t^{0.5}}{1 + \frac{k_r}{k_d} \cdot t^{0.5}} \quad (6)$$

#### *Estimation of the percolation threshold*

To determine the percolation threshold for PEO polymers with the selected  $M_r$  drug release from PEO binary PRTs (Table II) were evaluated with the standard paddle method (Apparatus II, VanKel Dissolution Apparatus, model VK 7000, USA,  $n = 3$ ) as described in section *Drug release study from PEO PRTs*. The polymer percolation threshold was defined

as the concentration of polymer in the matrix tablet at which drug release kinetics change significantly.

Drug release profiles were analyzed using the Higuchi equation 7 (38) and Korsmeyer-Peppas equation 8 (39):

$$Q = k_H t^{1/2} \quad (7)$$

$$Q = k t^m \quad (8)$$

where  $k_H$  and  $k$  are kinetic constants;  $m$  is an exponent indicating the release mechanism:  $m = 0.5$  indicates diffusion-controlled drug release and  $m = 1.0$  indicates relaxation-erosion-controlled drug release. Values between  $0.5 < m < 1.0$  indicate an anomalous (non-Fickian or both diffusion/relaxation) controlled drug release.

#### *Similarity factor calculation*

The drug release profiles of selected binary systems (TF X18, TF Y16, TF Z12 and TF X20, TF Y20, TF Z20) were compared using a similarity factor ( $f_2$ ), using Eq. 9. The number of dissolution sample times is sampled as  $n$ , and  $R_t$  represents the percent of drug dissolved in the reference at each sample point  $t$  and  $T_t$  in the test product. The drug release profiles of the two dissolution profiles are similar if  $f_2 \geq 50$  and dissimilar if  $f_2 < 50$ .

$$f_2 = 50 \log \left\{ \left[ 1 + \frac{1}{n} \sum_{t=1}^n (R_t - T_t)^2 \right]^{-0.5} \times 100 \right\} \quad (9)$$

#### *Statistical data analysis*

The reported values are means with standard deviations of experiments with at least three repetitions. A one-way analysis of variance (*t*-test) was used to analyze data and  $p < 0.05$  was considered as significant.

## RESULTS AND DISCUSSION

#### *Effect of tablet composition on gel relaxation times*

The relaxation times  $T_1$  and  $T_2$  were studied in: *i*) gels at known polymer concentrations of pure PEO polymers with three different  $M_r$  (low, medium, and high: TFs 1, 2, 3); *ii*) a mixture of medium-  $M_r$  PEO and PEG (TF 4); *iii*) pure PEG; and *iv*) a mixture of medium-  $M_r$  PEO, PEG, model drug, and other excipients (TF 6). The gels were prepared with purified water and a potassium phosphate buffer with a pH of 6.8. No differences between the relaxation times measured in gels prepared with water or potassium phosphate were observed, and therefore only the results of the relaxation times in gels prepared with a potassium phosphate buffer with a pH of 6.8 are shown in Fig. 1. At polymer concentrations below 80 %, two lines with mono-exponential  $T_1$  decay occurred, whereas at higher poly-

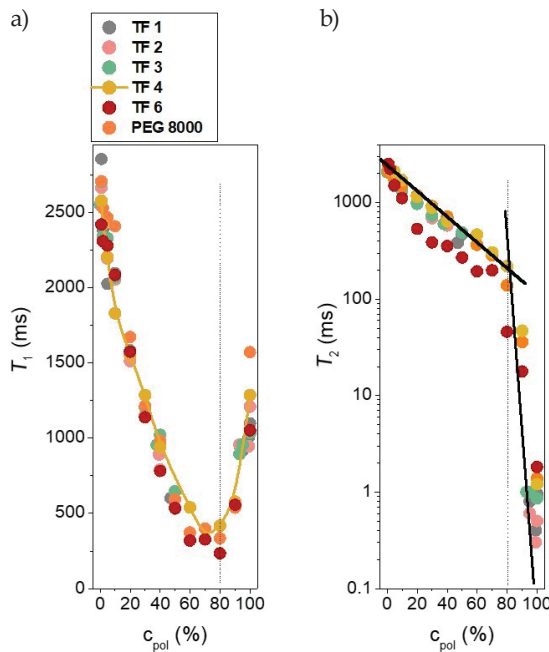


Fig. 1. Relaxation times (solid symbols): a)  $T_1$  and b)  $T_2$  for gels at different polymer ratios  $c_{\text{pol}}$  ( $m/m$ )  $\times$  100 % for TF 1, TF 2, TF 3, TF 4, TF 6, and PEG only in a potassium phosphate buffer with a pH of 6.8. Lines denote the position of  $T_1$  minimum and the break in the  $T_2$  slope.

mer concentrations one broad line with a double-exponential  $T_1$  decay was detected in the NMR spectra (data not shown). Different  $M_r$  or the presence of the excipients did not have any effect on  $T_1$  values (TFs 1–6). A decrease in  $T_1$  was observed when polymer concentration increased, exhibiting a minimum at  $c_{\text{pol}} \approx 80$  %, and increasing at higher concentrations (Fig. 1a).

The decay curves for  $T_2$  values were double-exponential. Both components of  $T_2$  decreased with increasing polymer concentration, and the decrease became significantly steeper at concentrations higher than 80 %. The  $T_2$  decrease was the consequence of more restricted proton mobility in gels with higher polymer concentrations. No differences among  $T_2$  values were observed among the different  $M_r$ , except for the gels containing PEO, PEG, model drug, and other excipients (TF 6), for which  $T_2$  values were significantly shorter (Fig. 1b).

MRI was used to visually and quantitatively monitor changes during tablet swelling. Penetration, swelling, and erosion fronts were evaluated using two different MRI methods: a 1D SPI pulse sequence was applied to determine medium penetration into the tablet and a 2D  $T_1$ -weighted spin-echo sequence to resolve the swelling front (the border between hydrated polymer in a glassy state and the gel) and erosion front (the border between the gel and bulk medium). The 2D spin-echo images at different swelling times for low- $M_r$  PEO are shown in Fig. 2a. The relaxation times  $T_1$  and  $T_2$  change with polymer concentra-

tion (Fig. 1), resulting in different signal intensity of gels with different polymer concentrations, which are seen as different MRI brightness. The dry tablet core was black on the MRI due to too short  $T_2$  of dry polymer. As the amount of medium in the gel increased, the  $T_2$  became longer, resulting in a brighter image. On the other hand, the medium signal was not very bright due to the long  $T_1$  and the use of the  $T_1$ -weighted spin-echo pulse sequence. The erosion and swelling fronts were determined from the signal intensity of 2D  $T_1$ -weighted spin-echo images. As can be seen from the  $T_2$  concentration dependence (Fig. 1b),

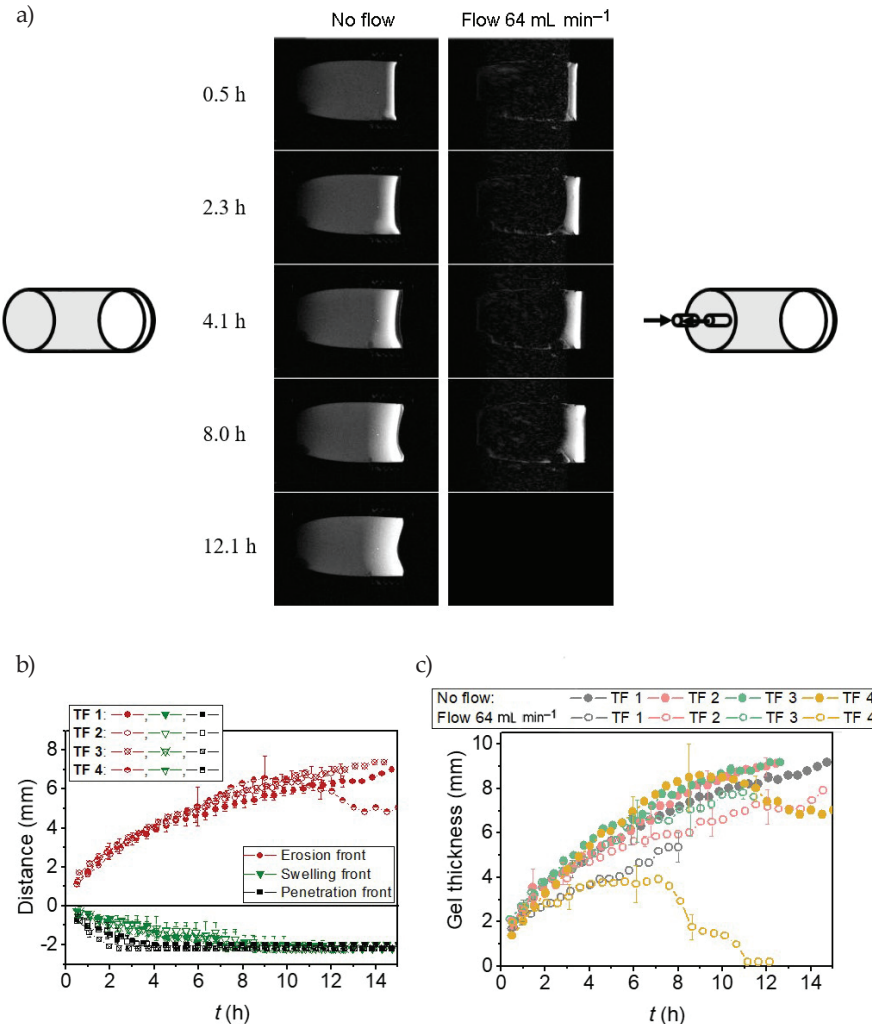


Fig. 2. a) MRI of TF 1 during swelling (left column without flow and right column with the flow of  $64 \text{ mL min}^{-1}$ ), TF 1, TF 2, TF 3, and TF 4; b) erosion, swelling, and penetration fronts; c) gel layer thickness without flow (solid symbols) and with  $64 \text{ mL min}^{-1}$  flow (open symbols).

the  $T_2$  steeply drops at phase transition from the glassy state to the gel state. The  $T_2$  value of concentrated gel just before the transition to the glassy state ( $T_2 > 100$  ms) is long enough to produce the spin-echo signal. In the glassy state, the  $T_2$  is much shorter ( $T_2 < 1$  ms) and no spin-echo MRI signal was observed. Therefore, the swelling front was determined at the position where the signal intensity vanishes and the erosion front at the position where the signal intensity starts to increase above the signal of the bulk medium. The penetration front was determined from the SPI signal intensity profile at the position where 1D SPI signal intensity increased above the signal intensity of the dry tablet core. The gel thickness was calculated as the difference between the erosion and swelling fronts.

#### *Effect of PEO M<sub>r</sub> on gel thickness under no-flow conditions*

First, the effect of the selected PEO on the swelling properties was investigated (Figs. 2b,c) under no-flow conditions. The differences in the penetration front between PEOs were noticed. Medium penetration is faster in high- $M_r$  PEO (TF 3; Fig. 2b), supporting literature data on faster water penetration into the matrix system due to its lower crystallinity (3). In the case of medium (TF 2) and low (TF 1)  $M_r$  PEOs there is higher crystallinity, preventing water from penetrating through the matrix system (11), and therefore the penetration is slower.

The swelling rate is independent of  $M_r$ , but some differences in erosion among different relative molecular masses have been observed. Erosion front expansion was slightly slower in the PEO with the lowest  $M_r$  (TF 1), resulting in a slightly thinner gel layer, especially at longer swelling times. The thinner gel layer in TF 1 results from the formation of a softer gel layer, which is more sensitive to erosion (2, 33). On the other hand, the gel layer in PEO tablets with higher  $M_r$  values (TFs 2 and 3) forms a gel less susceptible to erosion, resulting in a thicker gel layer (1, 3, 33).

#### *Effect of medium flow on gel thickness*

The effect of the medium flow on polymer swelling and gel erosion under mechanical stress, which is expected to be present under the *in vivo* conditions during tablet swelling, was studied for all three PEOs. The 2D spin-echo images of TF 1 containing the PEO with the lowest  $M_r$  during swelling with the highest medium flow of 64 mL min<sup>-1</sup> are shown in Fig. 2a. The medium signal was distorted owing to medium flow and consequently the movement of the medium during signal acquisition. On the other hand, the gel signal was undistorted because the gel was hard enough that the flow did not cause gel movement to such an extent that movements would cause image artefacts.

The data, thus, show that erosion front expansion drastically decreases when a medium flow of 64 mL min<sup>-1</sup> is applied to the PRTs, whereas the penetration and swelling fronts are not affected by the flow. Differences in the gel thicknesses measured under different mechanical stress conditions increase with swelling time (Fig. 2c).

The largest effect of the flow was observed in TF 1 with the lowest  $M_r$ , for which significantly thinner gel ( $\approx 5$  mm) was formed from the early beginning of the test (1 h) compared with the gel thickness of the same tablets swelling under the no-flow condition ( $\approx 9$  mm). Under stress conditions, the tablet completely disintegrated after 8 h (Fig. 2c). The differences in the gel thicknesses measured with and without flow were still significant but

smaller for the medium- $M_r$  formulation (TF 2), for which the gel thickness was the same for the first 4 h and became thinner ( $\approx 7$  mm) at later times compared to the gel thickness measured without flow ( $\approx 9$  mm). An insignificant difference was observed for the PEO with the highest  $M_r$  (TF 3), for which the gel became only slightly thinner after 10 h ( $\approx 8$  mm; Fig. 2c). Moreover, compared to low- $M_r$  PEO, TF 2 and TF 3 did not disintegrate during the test (12 h), showing a significant difference in gel layer strength.

At a flow rate of 64 mL min<sup>-1</sup>, the thinnest gel was formed during swelling of PEO with the lowest  $M_r$  followed by medium- $M_r$  PEO, and the thickest gel was formed during swelling of PEO tablets with the highest  $M_r$ . The results thus demonstrate that consistency of the gel layer depends on PEO  $M_r$  and that at applied mechanical stress the gel robustness increases with increasing  $M_r$ , supporting literature findings (1, 3, 40, 41).

#### *Effect of PEG addition on gel thickness*

To evaluate the impact of PEG on the swelling behavior of tablets composed of medium- $M_r$  PEO, TF 4 was used (Table I). Under static conditions, no significant differences between swelling properties of pure medium- $M_r$  PEO tablets (TF 2) and tablets with added PEG (TF 4) were observed in the first 10 h of swelling (after 4 h the swelling of the TF 4 tablets was slightly faster). However, after 10 h, the erosion of the TF 4 tablets had increased, resulting in a decrease of the gel thickness in contrast to pure medium- $M_r$  PEO (TF 2) tablets, for which the gel thickness increased up to 12 h (Fig. 2c). The impact of PEG on gel layer characteristics is even more pronounced when the gel thickness was measured with the medium flow. When mechanical stress was applied, the gel layer was significantly thinner ( $\approx 3$  mm) than in TF 2 tablets ( $\approx 7$  mm), and the tablet started to disintegrate after 7 h (Fig. 2c). Moreover, the gel layer thickness also decreased when compared to gel thickness under static conditions ( $\approx 9$  mm). The observed impact of the PEG is expected because the hydration of the pure PEG tablets in the medium was very fast and the tablet almost immediately disintegrated (data not shown). The results thus support and visualized the data regarding PEG chain domains, which are the same size as water, and therefore they work as a gel-enhancing agent, resulting in enhanced hydration and formation of a softer gel layer, which is more sensitive to erosion (27).

#### *Effect of tablet composition on gel thickness*

##### *No-flow conditions*

To evaluate the effect of PRT composition on gel thickness and swelling kinetics of PEO polymers representing a more realistic case in the development of PRTs, PEO polymers with selected relative molecular masses, model drug, PEG, and other excipients were formulated (TFs 5–7; Table I). Fig. 3a shows that for the lowest  $M_r$  PEO formulation (TF 5) the gel layer thickness increased with time and was only slightly thinner ( $< 1$  mm) for the first 5 h than in pure polymer tablets with the same  $M_r$  (TF 1). After 5 h, the gel thickness in TF 1 has continuously increased to form an approximately 9 mm gel layer, whereas the gel layer thickness of TF 5 became thinner ( $\approx 5.5$  mm) but constant after 6 h, showing that the rate of erosion and swelling was the same (Fig. 3a). Surprisingly, no differences in the gel layer thicknesses for the medium and the highest  $M_r$  PEO tablets without and with excipients were observed until 10 h, and after that, only a small reduction of the gel thick-

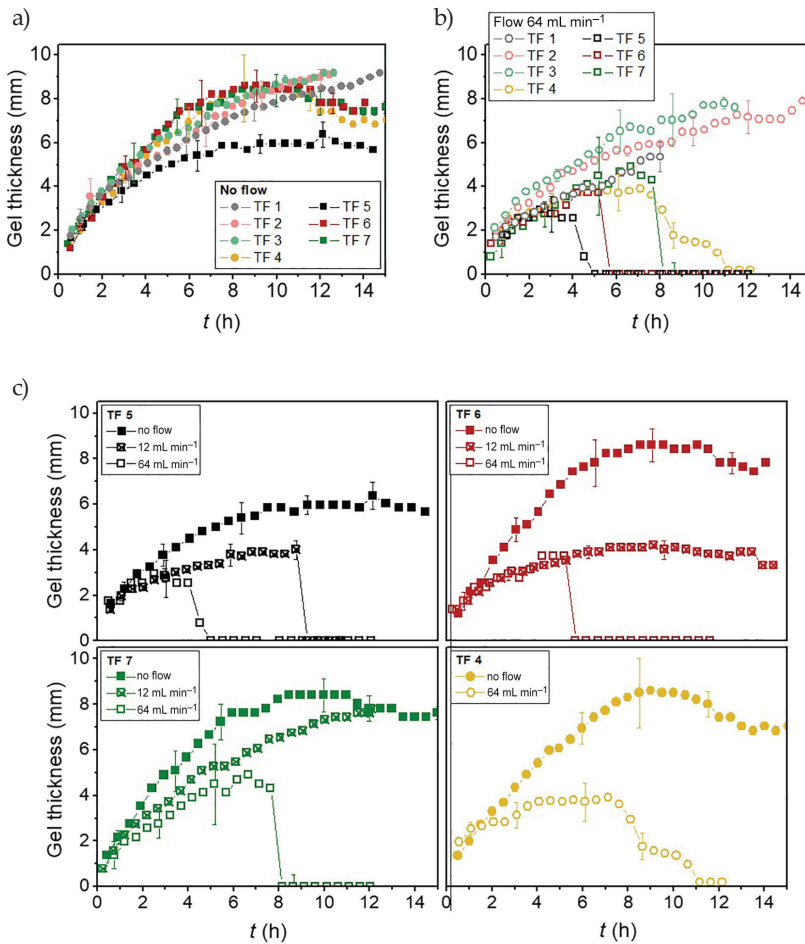


Fig. 3. Gel layer thicknesses for TFs 1–3, TF 4 (circles), and TFs 5–7 (squares). a) no flow; b) 64  $\text{mL min}^{-1}$  medium flow; c) comparison between the gel layer thicknesses without flow, with the flow of 12  $\text{mL min}^{-1}$ , and with the flow of 64  $\text{mL min}^{-1}$  for TF 4, TF 5, TF 6, and TF 7.

ness ( $\approx 1 \text{ mm}$ ) was detected. The results thus showed that the gel layer thicknesses do not significantly decrease when excipients are added to medium and high- $M_r$  PEO polymers when no mechanical stress is applied. In low- $M_r$  PEO, the gel layer reduction is significant, even under no-flow conditions.

#### Flow conditions

The effect of the addition of the excipients to PEO PRT was even more pronounced under flow conditions (Fig. 3b), confirming literature data (2, 33, 40). At the flow rate of 64  $\text{mL min}^{-1}$ , the greatest differences in gel layer thicknesses between tablets of the lowest  $M_r$  pure PEO (TF 1) and tablets of PEO with added excipients (TF 5) were observed. Gel thick-

nesses of pure polymer (TF 1) and polymer formulation with excipients (TF 5) were the same for the first 3 h ( $\approx 3$  mm). After that, the gel disintegration in TF 5 had increased with time, and the tablet had completely vanished after 5 h. On the other hand, in TF 1 the gel layer thickness had increased constantly up to 8 h. Similar differences were observed for medium- $M_r$  PEO containing excipients (TF 6), for which the gel layer was significantly thinner ( $\approx 3.5$  mm) compared to the gel layer ( $\approx 7$  mm) of the pure polymer (TF 2) and started to degrade after 5 h. For the highest  $M_r$  PEO formulation with excipients (TF 7), the gel layer was also thinner ( $\approx 4$  mm) than in TF 3 of the pure polymer ( $\approx 7$  mm), and its degradation started at approximately 8 h of swelling, whereas no gel degradation was observed in TF 3 at least for 12 h. The results confirmed that the addition of excipients into PRTs causes the formation of a more sensitive gel layer, which is more susceptible to erosion compared to PRT with pure polymer, regardless of polymer  $M_r$ .

For the medium- $M_r$  PEO, the impact of PEG only on the swelling was also studied. Differences in the gel thicknesses between TF 6 (containing the drug and other excipients) and TF 4 (containing only medium- $M_r$  PEO and PEG) were also observed. TF 6 degraded faster than TF 4. This shows that not only PEG but also other water-soluble additives enhance water penetration into PRT, disrupting intra-polymer interactions and enhancing the disentanglement of polymer chains, leading to faster erosion of PRT and consequently drug release (42), although the effect of the drug and other excipients was found to be much smaller than the effect of PEG. This supports prior reports that at a high PEG:PEO ratio erosion of the gel layer is determined by PEG concentration (27).

Additionally, the influence of mechanical forces (dynamic conditions) on gel layer thickness for TFs 4–7 was studied using two different flow rates: 12 and 64 mL min<sup>-1</sup> (Fig. 3c). In all cases, the gel layer thickness decreased with an increased flow rate due to enhanced erosion of PRTs. In the formulation with the lowest  $M_r$  PEO (TF 5), the gel thickness and the start of the erosion process correlate with the flow rate. Higher flow induces greater mechanical forces on the gel layer, causing faster degradation of the tablet compared to the lower flow, although the swelling rate for the first 2 hours was not affected. Moreover, for the medium- $M_r$  formulation (TF 6), a 64 mL min<sup>-1</sup> flow rate significantly increased matrix tablet degradation and the gel erosion process (5 h), whereas a 12 mL min<sup>-1</sup> flow was not strong enough to cause the total degradation of the gel layer formed. A constant thick gel layer of approximately 3.5 mm was formed at 12 mL min<sup>-1</sup> flow, showing a synchronized swelling and erosion process. Nevertheless, polymer (TF 7) with the highest-viscosity formed an approximately 8 mm thick gel resistant to mechanical stress caused by a flow of 12 mL min<sup>-1</sup>; that is, the gel thickness was approximately 1 mm thinner compared to the gel thickness measured under the no-flow condition. When the flow rate was increased to 64 mL min<sup>-1</sup>, gel erosion increased, resulting in a significantly more pronounced erosion process ending in a significantly thinner gel layer ( $\approx 4$  mm) and total disintegration of the tablet after 7 h.

It can, therefore, be concluded that after the addition of PEG, drug, and other excipients (TFs 4–7) to pure polymers (TFs 1–3) the gel thickness significantly decreases, which is even more pronounced under stress conditions. The most robust gel is formed with the highest  $M_r$  PEO (TF 7, Fig. 3b), confirming again that with increased  $M_r$  the gel layer consistency also increases due to a tighter connection between polymer chains. When only PEG was added to polymer (TF 4), the erosion process at a higher flow rate started 3 h later than in TF 6, confirming that other hydrophilic excipients (43) and the drug itself (44)

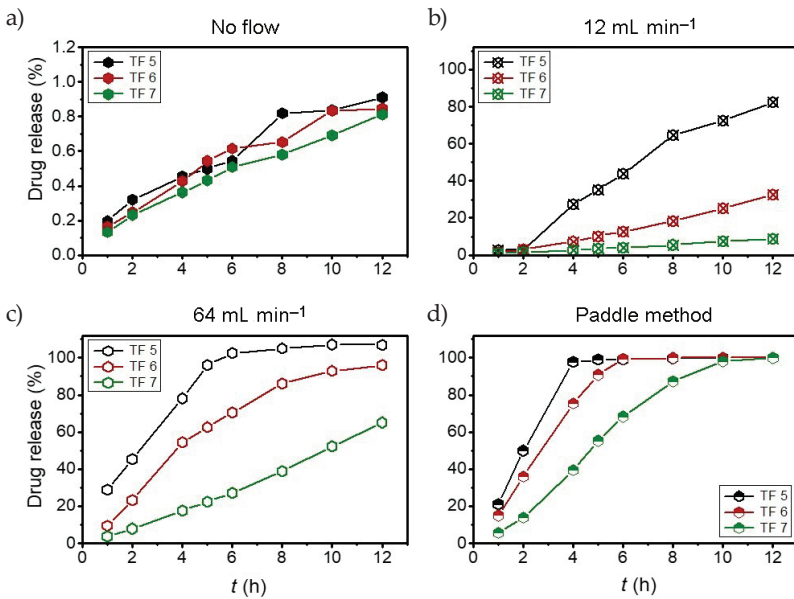


Fig. 4. Drug release profiles (symbols) for TFs 5–7 measured: a) without medium flow; b)  $12 \text{ mL min}^{-1}$  flow rate; c)  $64 \text{ mL min}^{-1}$  flow rate; d) standard paddle method.

also enhanced hydration of the matrix system. It is interesting to note that the swelling rate is the same for all formulations with added PEG or other excipients (TFs 4–7), but erosion is different and consequently, the tablet degradation depends on PEO's  $M_r$  (Fig. 3b). This shows that for the PEG-to-PEO ratio used, the erosion is defined by PEO's  $M_r$  (TFs 5–7), which is further increased by the addition of the drug and other excipients. The most significant reduction in the gel layer thickness was observed in the lowest  $M_r$  PEO studied. On the other hand, the next two  $M_r$  PEOs had exhibited a significantly lower reduction of the gel layer thickness after the addition of excipients, showing that due to rigid interactions among polymer molecules the gel is still strong and therefore robust to mechanical stress.

The different swelling kinetics of pure PEO tablets and PEO tablets with excipients are the result of the alteration of interactions between polymer chains (45), being more pronounced in low- $M_r$  PEOs. When highly soluble excipients are added into the formulation, the swelling/erosion rate changes (42). The presence of excipients broke the interactions and the chains started to unfold; erosion began and was synchronized with swelling, causing a constant gel layer thickness. Generally, during swelling, highly soluble excipients dissolve quickly before a tight gel layer is formed on the matrix surface. They absorb water and therefore help the medium penetrate into the inner matrix, leading to faster tablet hydration, and they accelerate initial swelling, which depends on the viscosity of the gel layer. Because PEG, drug, and other freely soluble excipients are added to the TFs, they significantly affect the formation of the gel layer, causing the same swelling rate but increase erosion in formulations (1, 3).

### Drug release from PEO PRT

Drug releases from TFs 5–7 were measured with no flow and at two different flow rates (12 and 64 mL min<sup>-1</sup>), as well as with the standard paddle method (Fig. 4). The drug release rates are significantly faster at higher flow rates, and the impact of the flow is more pronounced for the formulation containing the lowest  $M_r$  of PEO (TF 5 in Fig. 4a–c). The results show that drug release and its kinetics depend on the PEO  $M_r$  and mechanical stress applied to the matrix tablets.

### Correlation between drug release kinetics and gel layer thickness

To evaluate the diffusion and erosion contribution to drug release, drug release profiles and gel thicknesses measured under the same conditions were fitted using Eqs. 1 and 2, and the relative effect of diffusion and erosion mechanisms on drug release were determined using Eqs. 5 and 6, respectively. The parameters obtained by the fittings are presented in Table III and Fig. 5. Parameter  $A$ , which depends on the rate of chain relaxation and swelling (representing the diffusion impact on drug release), is independent of flow rate and PEO  $M_r$ , indicating that neither the flow rate nor polymer  $M_r$  change the polymer swelling. Parameter  $B$ , which describes the gel erosion, increases with increasing flow rate as well as with decreasing PEO  $M_r$ . The parameter  $\beta$ , which depends on drug equilibrium volume fractions at gel-medium interface  $S$  ( $v_{deq}$ ) and at glassy-gel interface  $R$  ( $v_d^*$ ), also depends on PEO  $M_r$  and on flow rate. It increases with increasing mechanical stress for all relative molecular masses. When drug release and gel thicknesses were measured without the flow,  $v_{eq}$  was independent of  $M_r$  (Table III), confirmed also with dissolution data (Fig. 4a). Under no mechanical stress, gel erosion is very small (*i.e.*, only 1 %), and the main release mechanism is drug diffusion through the gel layer, which can also be seen from the diffusion and erosion contribution obtained by simultaneously fitting the gel thicknesses and drug releases during tablet hydration (Figs. 6a and 5b, Table III). Furthermore, a difference in gel layer thickness occurred between TF 5 formulations containing a lower PEO  $M_r$  ( $\approx 6$  mm) and between TF 6 and 7, containing higher  $M_r$  ( $\approx 8$  mm). Upon increased mechanical stress during tablet swelling,  $v_{eq}$  increased and became  $M_r$ -dependent; that is, it decreased with increasing  $M_r$ , confirming dynamic condition drug release results (Fig. 4b–d). This demonstrates that, when the mechanical stress was absent, the equilibrium drug concentrations at swelling and erosion fronts were the same for all PEOs, but at higher shear forces the gel of PEO with lower  $M_r$  was weaker and it eroded faster, also causing higher drug concentration at the erosion front. The values of the delay time  $t_0$  (Table III) were non-zero only at a flow rate of 12 mL min<sup>-1</sup> ( $t_0 = 1.6$  h for TF 5, 1.1 h for TF 6, and 1.0 h for TF 7) and at 64 mL min<sup>-1</sup> flow in PEO tablets with the highest  $M_r$  ( $t_0 = 0.7$  h for TF 7). This implies that under such flow conditions large parts of the gel were detached from PRT-hydrated gels and a certain period of time was needed for the drug to diffuse or erode out of it. At 64 mL min<sup>-1</sup> flow, the mechanical forces were strong enough that they broke the eroded medium- and low- $M_r$  PEO gel so quickly that the delay time could not be detected. On the other hand, they were not strong enough for total erosion of the gel parts removed from the gel layer formed with the PEO with the highest  $M_r$ .

The relative contributions of diffusion and erosion mechanisms to drug release at different hydration times are shown in Figs. 5a,b. The results demonstrate that under no-flow conditions diffusion is the main release mechanism for all molecular masses at all time

*Table III. Values of fitting parameters determined from gel thicknesses and drug releases for test formulations (TF) 5–7*

Flow (mL min <sup>-1</sup> )	A (mm <sup>2</sup> h <sup>-1</sup> )	B (mm h <sup>-1</sup> )	v <sub>eq</sub>	t <sub>0</sub> (h)	k <sub>d</sub> (1/h <sup>0.5</sup> )	k <sub>r</sub> (1/h)	k <sub>d</sub> /k <sub>r</sub> (h <sup>0.5</sup> )
TF 5							
No flow	5.8	0.8	0.001	0.0	0.0015	0.0004	4.2
12	5.7	1.8	0.057	1.6	0.0960	0.0520	1.8
64	6.0	2.1	0.100	0.0	0.1700	0.1030	1.7
TF 6							
No flow	6.0	0.5	0.001	0.0	0.0017	0.0002	7.2
12	5.8	1.4	0.022	1.1	0.0370	0.0160	2.3
64	6.0	1.6	0.070	0.0	0.1210	0.0570	2.1
TF 7							
No flow	6.1	0.6	0.001	0.0	0.0014	0.0002	6.3
12	5.8	0.7	0.010	1.0	0.0170	0.0033	5.2
64	6.0	1.1	0.048	0.7	0.0800	0.0280	3.0

A – Fickian diffusion, B – erosion contribution, v<sub>eq</sub> – medium equilibrium volume fractions at swelling interface, t<sub>0</sub> – delay time, k<sub>d</sub> – diffusion rate constant, k<sub>r</sub> – erosion rate constant

points measured and correlates well with gel layer thickness under the same conditions ( $R^2 = 0.91$ ). At applied flow, the diffusion mechanism dominated drug release at the beginning, but later the erosion mechanism prevailed in the lowest and medium- $M_r$  PRTs (TFs 5 and 6). The transition from diffusion-to erosion-dominated drug release occurred 1 h later when a flow rate of 12 mL min<sup>-1</sup> was applied (Fig. 5b). In the tablets with the highest  $M_r$  (TF 7), the effect of 12 mL min<sup>-1</sup> flow rate is insignificant compared to the static condition, and the diffusion mechanism dominates for the first 13 h. The effect of flow on erosion was observed at a flow rate of 64 mL min<sup>-1</sup>, at which the erosion mechanism prevailed at approximately 8 h. The dominant release mechanism depends on the gel layer properties. When the gel layer is tough enough to withstand mechanical stress, diffusion is predominant; in contrast, when the gel layer is weaker, erosion overcomes the diffusion mechanism. The gel layer properties mostly depend on the polymer characteristics, mainly on its viscosity, concentration, and additives added, affecting the intrapolymer interactions (46).

Moreover, a good correlation was established between drug release profiles gained by the standard paddle method and gel thicknesses ( $R^2 = 0.91$ ), confirming previously reported data that increased  $M$  forms a thicker and more robust gel layer, resistant to mechanical stresses.

A correlation between the previously reported network solution concentration (47) and the diffusion coefficient ( $A$ ) under the no-flow condition was found ( $R^2 = 0.95$ ), confirming the formation of a robust gel at a lower concentration for a polymer with a higher  $M_p$ , for which diffusion makes a larger contribution to drug release. Moreover, a good correlation ( $R^2 = 0.96$ ) between the erosion coefficient ( $B$ ) and gel thickness under flow conditions of 64 mL min<sup>-1</sup> was also established, confirming that erosion is reduced with increased gel layer thickness.

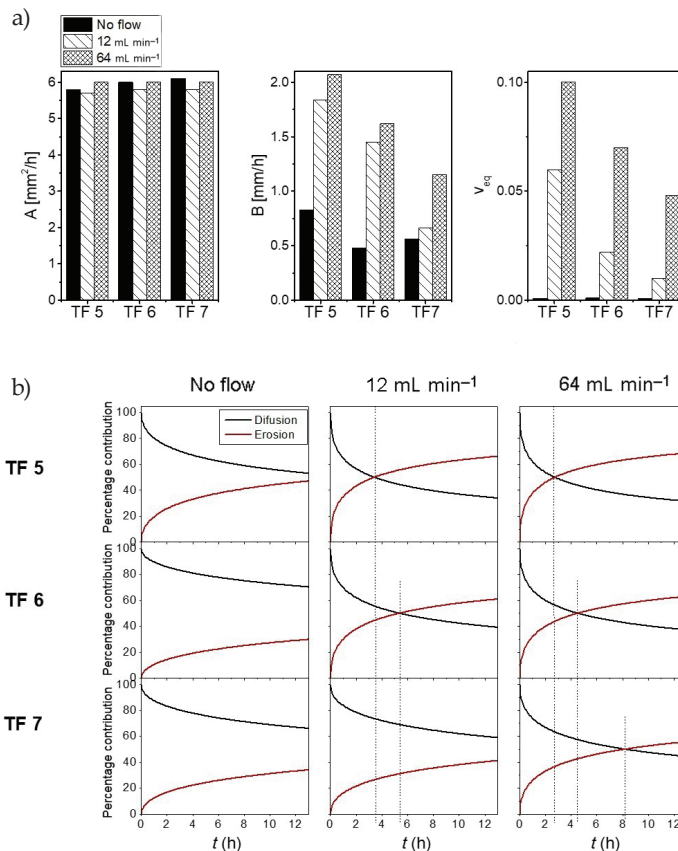


Fig. 5. a) Parameters  $A$ ,  $B$ , and  $v_{eq}$  obtained by fitting the time dependencies of the gel layer thicknesses and drug release kinetics using Eqs. 1 and 2 for TF 5, TF 6, and TF 7 at different flow rates; b) the diffusion and erosion contributions to drug release determined from fitting parameters and calculated by Eqs. 5 and 6 at different swelling times.

This conclusion is also supported by a good correlation between the reported rheological Young's modulus ( $E_r$ ) (47) and  $B$  in the case of increased mechanical stress ( $R^2 = 1.00$  for 12 mL min<sup>-1</sup> and  $R^2 = 0.98$  for 64 mL min<sup>-1</sup>). This confirms that when a more viscous gel layer is formed (PEO with a higher  $M_r$ ) the erosion is lower, leading to slower drug release mainly through diffusion.

At the same time, a good correlation ( $R^2 > 0.95$ ) was also established between gel thickness determined at a flow rate of 64 mL min<sup>-1</sup> and drug release under the same conditions in the first 5 h regardless of PEO  $M_r$ . After 5 h the correlation had decreased with time (Fig. 5b) due to the predominant erosion mechanism, resulting in uncontrolled destruction of the gel layers. As a result, all three PEO tablets had disintegrated in at least 8 h, leading to a faster drug release (1, 2, 33, 40, 44). The same effect can also be gained with lower polymer concentrations in the matrix tablets (33, 48).

### Estimation of the percolation threshold

Taking into consideration the percolation theory, different drug release behavior in relation to polymer concentration due to the formation of inherent gel layers is expected (16). In this study, initial binary systems of the model drug (BCS III) and PEO polymers with different  $M_r$  and different polymer ratio (% of polymer) were investigated (Table II). For medium- $M_r$  PEO, a comparison between binary (TF Y10–Y30; Table II) and multicomponent systems (TF 6; Table I) was also performed in order to understand the impact of the excipients (TF 6a; Table I) and tablet shape (TF 6b; Table I) on drug release (*i.e.*, connected to its surface-to-volume ratio). It should be noted that drug solubility can affect drug release (16, 42, 44, 49), but because the same model drug (BCS III) was used for all selected binary systems (X, Y, Z) its solubility effect on drug release was the same in all cases, and therefore only the polymer  $M_r$  effect was observed.

During the research, 40 batches of tablets with different PEOs were prepared using up to 17 different polymer and model drug ratios ranging from 10 to 90 %. Only concentrations near percolation thresholds are presented in detail here (Fig. 6 and Table IV).

Based on drug release profiles (Fig. 6), a significant change in the % of the released drug was observed between 16 and 18 % of the lowest  $M_r$  PEO concentration (TFs X, Fig. 6a). For medium- $M_r$  PEO (TFs Y, Fig. 6b), a change in release profiles was observed between

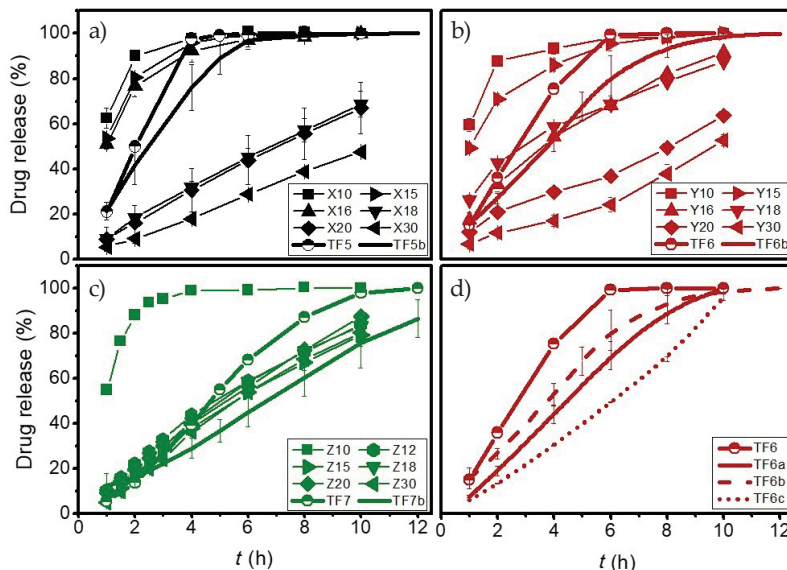


Fig. 6. Drug release profiles using the paddle method from: a) binary systems (X10–X30) and multicomponent systems of low- $M_r$  PEO with round (TF 5) and oval (TF 5b) tablet shapes; b) binary systems (Y10–Y30) and multicomponent systems with medium- $M_r$  PEO with round (TF 6) and oval (TF 6b) tablet shapes; c) binary systems (Z10–Z30) and multicomponent systems with high- $M_r$  PEO with round (TF 7) and oval (TF 7b) tablet shapes; and d) medium- $M_r$  PEO tablets (TF 6, round and TF 6b, oval) with different proportions of PEO (TFs 6a–6c).

Table IV. Higuchi ( $k_h$ ) and Korsmeyer-Peppas (k) kinetic constants, with corresponding exponent m indicating the release mechanism, and determination coefficient ( $R^2$ ) of binary test formulations (TF) X, Y and Z and multicomponent TFs (TF 5, TF 6 and TF 7)

TF	% PEO (m/m)	Higuchi equation		Korsmeyer-Peppas equation		
		$k_h$ (% min <sup>-0.5</sup> )	$R^2$	k (% h <sup>-1</sup> )	m	$R^2$
X10	10	1.902	0.67	17.376	0.324	0.86
X15	15	2.529	0.77	9.894	0.422	0.94
X16	16	2.767	0.85	8.857	0.431	0.96
X18	18	3.535	0.99	0.311	0.843	1.00
X20	20	3.502	0.99	0.229	0.890	1.00
X30	30	2.561	0.97	4.452	1.032	1.00
TF 5	27	4.722	0.80	1.291	0.693	0.99
Y10	10	2.026	0.72	21.504	0.285	0.92
Y15	15	2.933	0.91	8.440	0.437	0.97
Y16	16	4.446	1.00	0.748	0.779	0.99
Y18	18	3.537	0.99	3.069	0.536	0.98
Y20	20	2.878	0.96	0.654	0.702	0.98
Y30	30	2.558	0.90	0.141	0.904	0.96
TF 6	27	5.487	0.91	0.325	0.920	1.00
Z10	10	1.996	0.58	3.157	0.701	0.98
Z12	12	4.456	1.00	0.298	0.888	0.99
Z15	15	4.311	1.00	0.180	0.959	0.99
Z18	18	4.594	1.00	0.191	0.961	0.99
Z20	20	4.722	0.99	0.151	1.011	1.00
Z30	30	4.675	0.99	0.047	1.220	1.00
TF 7	27	6.041	0.99	0.284	0.978	0.99

15 and 16 % of polymer concentration. For the highest  $M_r$  PEO (TFs Z, Fig. 6c), a significant change in drug release profile was detected between 10 and 12 % of the polymer. Percolation thresholds were set as follows: for low- $M_r$  PEO at 18 % of polymer concentration, for medium- $M_r$  PEO at 16 %, and for high- $M_r$  PEO at 12 %. All set concentration thresholds are lower than previously estimated, confirming that the general recommendation (50) of more than 20 % PEO polymer in the matrix formulation is well set in the case of binary systems.

To confirm the percolation thresholds of binary mixtures based on drug release studies (Fig. 6), kinetic constants were also calculated using Eq. 7 and 8. The kinetic data (Table IV) confirmed the PEO percolation threshold concentrations. Above set percolation

thresholds, the drug release rate is controlled by diffusion through a fully hydrated gel layer. Diffusion was detected by a good fit of the drug release kinetics to the Higuchi equation ( $R^2 \geq 0.99$ ). On the other hand,  $m$  values of the Korsmeyer-Peppas equation being close to 0.8 indicated anomalous diffusion (39). Below the percolation threshold, a sufficient gel layer is not formed, leading to uncontrolled drug release, resulting in a significant increase of the Korsmeyer-Peppas constant ( $k$ ) (Table IV) for all selected PEOs.

The results thus show that the percolation threshold depends on the PEO  $M_r$  ( $R^2 = 1.00$ ). According to that, a good correlation ( $R^2 = 0.98$ ) was established between the previously determined concentrated network solution for selected PEOs (47) and the determined percolation threshold concentrations.

Gel layer robustness depends on PEO's  $M_r$  and the start of the erosion process, which was also confirmed with a correlation study ( $R^2 = 0.96$ ) between the erosion coefficient ( $B$ ) at  $64 \text{ mL min}^{-1}$  (Table III) and set percolation thresholds. The difference occurred due to different polymer characteristics. Different polymer  $M_r$  microstructures define their hydration rate and viscosity, leading to differences in the velocity of drug release and faster drug release from the TFs with a lower  $M_r$  due to the formation of the softer gel layer.

It should be considered that, in addition to polymer concentration and its viscosity, polymer particle size distribution, excipients, drug concentration, and solubility (16) can also affect the percolation threshold. Because usually more than one excipient is used for the formation of PRTs, a binary system's percolation threshold results should be interpreted carefully.

When comparing binary systems (TFs X-Z; Table II) with multicomponent systems (TFs 5–7; Table I) with the same size and shape, it can be concluded that for all multicomponent TFs investigated anomalous drug release kinetics were detected (Korsmeyer-Peppas  $0.5 < m < 1$ ; Table IV) as a result of drug diffusion and matrix erosion events. Drug release rates (Fig. 6a–c) from PEO TFs containing 27 % polymer (TF 5, 6, and 7) changed with the addition of water-soluble excipients compared to a binary system near the same polymer concentration (30 %) of the same PEO  $M_r$  (TFs X–Z, Fig. 6).

To confirm the importance of well-set percolation thresholds, different medium- $M_r$  PEO ratios (23, 27, and 35 %) in multicomponent formulations were evaluated (TFs 6a–6c; Table I). The similarity factor ( $f_2$ ) between selected multicomponent formulations was calculated using Eq. 9. Comparable drug release ( $f_2 = 52$ ) for the TFs containing 23 % (TF 6a) and 27 % (TF 6b) of medium- $M_r$  PEO can be found. On the other hand, drug release from a multicomponent system containing 35 % medium- $M_r$  PEO (TF 6c; Fig. 6d) is significantly slower ( $f_2 = 34$ ). These data show that the percolation threshold for the selected intermediate- $M_r$  PEO multicomponent system is above 27 % and is much higher than in the binary system of the same PEO  $M_r$  (16 %). The results support the literature data that the addition of excipients enhances drug release (1, 3, 42, 44, 49) and significantly affect the polymer percolation threshold and that the proposed percolation threshold for PEO polymers of 20 % (50) is too low in selected multicomponent PEO formulations. These results support the theory that the percolation threshold for multicomponent systems should be precisely determined during formulation development because the formation of a robust gel layer is crucial for ensuring controlled drug release (19). If the percolation threshold is not reached, the drug release from such PRTs can be uncontrolled and quite variable. Moreover, the outcome from dissolution results strengthens the research data that the gel layer

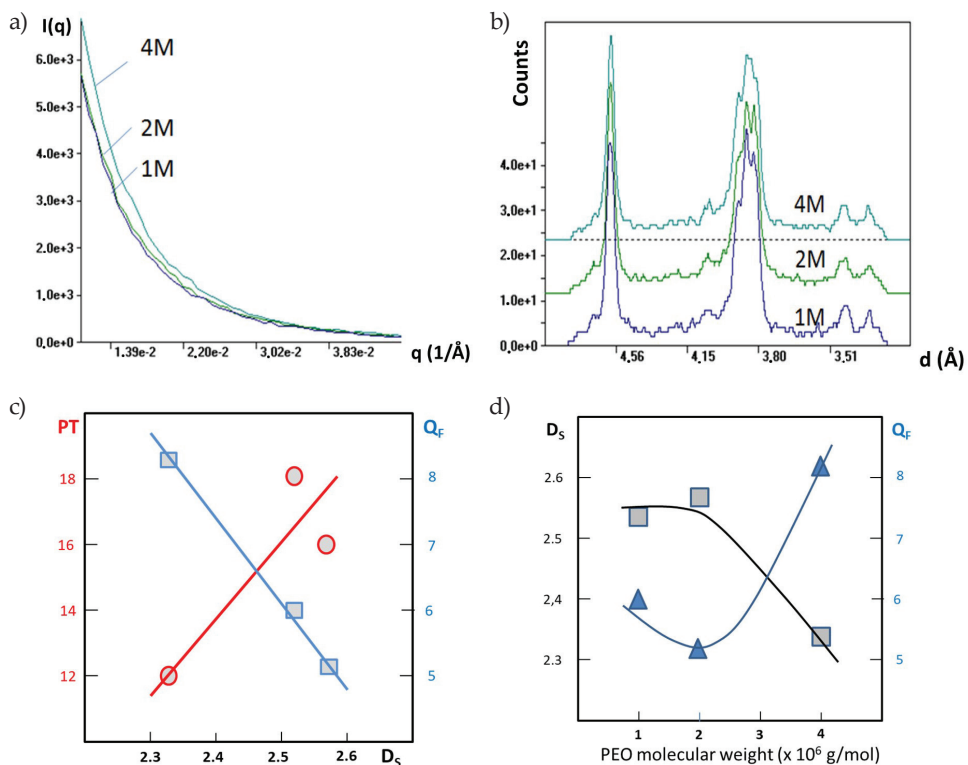


Fig. 7. Overlays of: a) SAXS; b) WAXS profiles of PEO powders with low (1M), medium (2M), and high (4M)  $M_r$ ; The plots of: c) percolation threshold (PT, circle) and the ratio of the heat of coalescence to the heat of fusion ( $Q_F$ , diamond) *vs.* surface fractal dimension ( $D_s$ ) of different PEOs; d)  $D_s$  (square) and  $Q_F$  (the heat of coalescence to the heat of fusion\*100) (triangle) *vs.* surface  $M_r$  of PEO.

robustness can be increased with a higher polymer proportion, resulting in a more uniform gel layer and a better-controlled drug release (3, 43, 48).

When comparing multicomponent systems with the same mass and composition but with different shapes (TFs 5, 5b; 6, 6b; and 7, 7b), it was concluded that the shape of the tablet as well as the polymer proportion significantly ( $f_2 < 50$ ) affect the drug release kinetics (Fig. 7). Drug release from a round tablet is faster than from an oval one due to its greater surface area, confirming the same literature data (51). These results indicate that the PEO concentration threshold differs between its  $M_r$  formulation composition (Table I, Fig. 6a-d), and tablet shapes (Table I, Fig. 6a-c).

The results confirmed that percolation theory is directly connected to the polymer  $M_r$  and composition and shape of a tablet. At the same time, they show that the percolation threshold for a binary system is not a good indicator of the percolation threshold of a multicomponent system. Finally, they showed that the general proposed minimal critical PEO polymer concentration limit (20–30 %) (50, 52, 53) depends on several factors and should be well set during the development of PRTs.

Therefore, it is crucial to consider all these factors during PRT development. Notably, higher polymer concentration must be applied in a multicomponent formulation in order to gain a robust PRT, ensuring controlled drug release compared to the binary system.

Relationship of PEO thermo-physical properties and nanostructure parameters to percolation threshold of drug loading

To better understand the difference between selected polymers at the molecular level, SAXS and WAXS analyses of the PEO powders were performed. Figs. 7a,b show the overlay of powder SAXS and WAXS profiles of three PEOs obtained at room temperature. Examining the SAXS profiles, samples with low and medium  $M_r$  show almost identical patterns, whereas the sample with a higher  $M_r$  differs significantly in the low-angle part, qualitatively indicating larger nanostructural features in the solid state. On the other hand, the identical Bragg peak positions in the WAXS patterns confirm the very similar crystal structure among all the selected PEOs. Furthermore, the relative peak intensities of the Bragg peaks with respect to the diffuse background of an amorphous halo (data not shown) reveal a comparable degree of crystallinity in the PEOs of different molecular masses, confirming prior data obtained through DSC or X-ray diffraction (47, 54).

The qualitative analysis of the SAXS patterns shows systematic differences between selected PEOs in the surface fractal dimension ( $D_s$ )<sub>s</sub> at the nanoscale (*i.e.*, between 1 and 100 nm). The  $D_s$  values were derived as the slope of the logarithmic plot of scattering intensity versus the scattering vector (34). As seen in Fig. 7c, the SAXS-derived  $D_s$  values apparently correlate with the percolation threshold concentration of the composition-

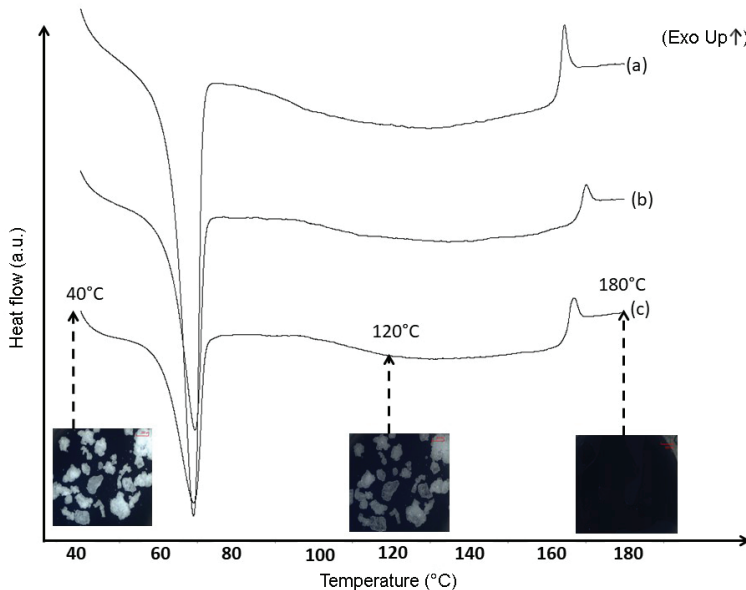


Fig. 8. An overlay of DSC thermograms of PEOs of selected molecular masses: a) low; b) medium; c) high. The micrographs at 40 and 120 °C are shown to illustrate the intactness of polymer particles beyond the melting point and below the flow transition temperature.

-dependent change of the drug release profile of PEOs with different molecular masses. A correlation between fractal properties and percolation threshold has also been suggested in terms of permeability through the matrix network (55).

In Fig. 8, the thermograms of semi-crystalline PEOs of different molecular masses comprise the melting transition of crystalline fractions at 69 °C, which is in agreement with the range reported in the literature (56). The glass transitions of the amorphous fractions of PEO are reported between –50 and –57 °C (57). Therefore, the supercooled liquid phase of amorphous PEO fractions is embedded between the ensembles of the crystalline domains. Interestingly, the thermograms show a small but distinct exothermic event at around 164–170 °C, which is 95–100 °C above the melting point. To our knowledge, such thermal transitions in PEOs have not been reported in the literature. Thermal microscopy of the PEO powders was used to visually observe the events related to this peculiar thermal signature. As seen in the micrographs at 40 and 120 °C, PEO particles remain intact and uncoalesced even at a temperature much above the melting temperature. They were also more transparent (due to the melting of the crystalline fraction). However, particles were observed to transiently coalesce across the temperature region of the exotherm. This suggests that the exotherm represents the heat of coalescence, and the corresponding temperature is attributable to the onset of the viscous flow transition of anisotropic melt to the isotropic phase. The ratios of the heat of coalescence to the heat of fusion (QF) for different PEOs are presented in Fig. 7d. From the plots, a clear correlation of D<sub>s</sub> and QF was observed. The opposite relations of PT and QF to D<sub>s</sub> suggest that the thermal plasticization propensity of the PEO structures can be considered analogously to the water-induced plasticization process during gel formation.

Finally, the qualitative differences between selected PEO polymers were detected using thermal microscopy between 120 and 170 °C, confirming that the exothermic peak is related to the process of particle coalescence of fully X-ray amorphous grains, which is a unique feature for polymers with melt memory. Furthermore, the SAXS results defined differences between selected PEO polymers in D<sub>s</sub>, indicating polymer complexity due to the corrugated nanostructure of the polymeric particle surfaces. This is possibly related to the difference in the extents and modes of lamellar folding for PEO crystals and the embedded degree of heterogeneity of their amorphous states. Although not widely exploited so far for PEOs, it has been argued in the literature that D<sub>s</sub> values correlate with the drug loading capacity in the nanoparticles based on PEG-PLA copolymer (58). Ma *et al.* recently reported an interesting study of the evolution of a fractal parameter obtained by SAXS during drug delivery from a silica-polymer based core-shell structure (59). Therefore, with increased polymer M<sub>r</sub>, the surface roughness of polymer particles is lower, defining higher resistance to diffusion and consequently lower drug release from such systems.

The results thus show that PRT characteristics depend on the polymer's attributes, which are defined by its molecular nature. This study has, therefore, systematically indicated how nanostructural differences of PEO polymers affect the final quality of PRTs. It shows that the differences in nanostructure between PEO polymers with different M<sub>r</sub> define their characteristics during swelling, a feature additionally quantified by MRI. With several fundamental correlations, it shows that understanding PEO polymer properties at the molecular (nanostructural) level can be a good way to predict the final formulation behavior. This study managed to connect data at the molecular level so that is applicable to data at the bulk level. The data thus show that from molecular level polymer characteristics it is possible to predict formulation behavior at the bulk level.

## CONCLUSIONS

This study presents a structured and detailed insight into the behavior of PEO polymers at different levels. Differences observed at the microstructural level (SAXS and thermal analysis) between different PEO molecular masses are reflected at the macroscopic level (MRI analysis), resulting in  $M_r$ -dependent hydration rate as well as the gel consistency. The thickest and strongest gel is formed in the matrix formulation composed of PEO with the highest  $M_r$ . The systematic evaluation of mechanical stresses' impact on gel thickness during tablet swelling showed that differences depend on the PEO molecular masses. SAXS detected the difference in nanostructure between the high  $M_r$  PEO and the other two PEOs. The ratio of the heat of coalescence to the heat of fusion for different PEOs obtained through DSC correlated with the polymer nanoscale surface fractal dimension, representing a novel approach to qualitative separation of PEO polymers with different molecular masses. According to differences in the nanoscale surface dimension, the diffusion rate in high- $M_r$  PEO is smaller compared to PEOs with a lower  $M_r$ , explaining the differences in their drug release rates.

The diffusion and erosion contributions to drug release were calculated in order to confirm the experimental results. This showed that under no-flow conditions the main release mechanism for all selected PEOs through the gel layer is drug diffusion. Under mechanical stress, the diffusion mechanism dominates at the beginning, but later the erosion mechanism prevails, showing higher resistance in higher  $M_r$  PEO.

Several good correlations between results gained at the molecular, film, and bulk levels were established. Based on the correlations obtained, it can be assumed that the drug release rate depends on gel thickness ( $R^2 = 0.91$ ) and is closely connected to the erosion coefficient ( $B$ ) ( $R^2 = 0.96$ ) and polymer rheological characteristics.

For selected PEO  $M_r$  binary systems, the percolation thresholds were set to 12 % for high, to 16 % for medium, and to 18 % for low  $M_r$  PEOs. Furthermore, the addition of water-soluble excipients and increased tablets' surface area raised the percolation threshold concentration above 27 % in the medium  $M_r$  PEO. As an innovative approach for percolation threshold prediction, a good correlation ( $R^2 = 0.98$ ) between the reported concentrated network solutions and set binary percolation thresholds was established.

*Acknowledgments.* – The authors are grateful to the Slovenian Research Agency and Department of Pharmaceutical Technology, University of Ljubljana for supporting this study (P1-0189, Pharmaceutical technology: from drug delivery systems to therapeutic outcomes of medicines in children and the elderly). Special thanks to our late beloved professor Saša Baumgartner for all her contributions to the application of MRI for investigating matrix tablets.

*Abbreviations.* – DSC – differential scanning calorimetry, MR – magnetic resonance,  $M_r$  – relative molecular mass, MRI – magnetic resonance imaging, NMR – nuclear magnetic resonance, PEO – polyethylene oxide, SAXS – small-angle X-ray scattering, WAXS – wide-angle X-ray scattering.

## REFERENCES

1. C. J. Kim, Drug release from compressed hydrophilic POLYOX-WSR tablets, *J. Pharm. Sci.* **84** (1995) 303–306; <https://doi.org/10.1002/jps.2600840308>
2. L. Maggi, R. Bruni and U. Conte, High molecular weight polyethylene oxides (PEOs) as an alternative to HPMC in controlled release dosage forms, *Int. J. Pharm.* **195** (2000) 229–238; [https://doi.org/10.1016/S0378-5173\(99\)00402-0](https://doi.org/10.1016/S0378-5173(99)00402-0)

3. A. Apicella, B. Cappello, M. A. Del Nobile, M. I. La Rotonda, G. Mensitieri and L. Nicolais, Poly(ethylene oxide) (PEO) and different molecular weight PEO blends monolithic devices for drug release, *Biomaterials* **14** (1993) 83–90; [https://doi.org/10.1016/0142-9612\(93\)90215-N](https://doi.org/10.1016/0142-9612(93)90215-N)
4. P. Draksler, D. Lamešić and B. Janković, Physical properties of polymers used in pharmacy – Do we really know them?, *Farm. Vestn.* **67** (2016) 265–272.
5. B. Hammouda, D. L. Ho and S. Kline, Insight into clustering in poly(ethylene oxide) solutions, *Macromolecules* **37** (2004) 6932–6937; <https://doi.org/10.1021/ma049623d>
6. D. L. Ho, B. Hammouda and S. R. Kline, Clustering of poly(ethylene oxide) in water revisited, *J. Polymer Sci. Part B: Polymer Physics* **41** (2002) 135–138; <https://doi.org/10.1002/polb.10340>
7. D. Rivero, L. M. Gouveia, A. J. Müller and A. E. Sáez, Shear-thickening behavior of high molecular weight poly(ethylene oxide) solutions, *Rheol. Acta* **51** (2011) 13–20; <https://doi.org/10.1007/s00397-011-0569-7>
8. A. S. Hoffman, The origins and evolution of “controlled” drug delivery systems, *J. Control. Release* **132** (2008) 153–163; <https://doi.org/10.1016/j.jconrel.2008.08.012>
9. Q. T. Nguyen, E. Favre, Z. H. Ping and J. Néel, Clustering of solvents in membranes and its influence on membrane transport properties, *J. Memb. Sci.* **113** (1996) 137–150; [https://doi.org/10.1016/0376-7388\(95\)00219-7](https://doi.org/10.1016/0376-7388(95)00219-7)
10. J. H. Park and Y. H. Bae, Hydrogels based on poly(ethylene oxide) and poly(tetramethylene oxide) or poly(dimethyl siloxane). II. Physical properties and bacterial adhesion, *J. Appl. Polym. Sci.* **89** (2003) 1505–1514; <https://doi.org/10.1002/app.12217>
11. S. K. Mallapragada and N. A. Peppas, Crystal dissolution-controlled release systems: I. Physical characteristics and modeling analysis, *J. Control. Release* **45** (1997) 87–94; [https://doi.org/10.1016/S0168-3659\(96\)01549-0](https://doi.org/10.1016/S0168-3659(96)01549-0)
12. S. K. Mallapragada, N. A. Peppas and P. Colombo, Crystal dissolution-controlled release systems. II. Metronidazole release from semicrystalline poly(vinyl alcohol) systems, *J. Biomed. Mater. Res.* **36** (1997) 125–130; [https://doi.org/10.1002/\(SICI\)1097-4636\(199707\)36:1<125::AID-JBM15>3E3.0.CO;2-H](https://doi.org/10.1002/(SICI)1097-4636(199707)36:1<125::AID-JBM15>3E3.0.CO;2-H)
13. B. Hammouda, Solvation characteristics of a model water-soluble polymer, *J. Polym. Sci. Part B Polym. Phys.* **44** (2006) 3195–3199; <https://doi.org/10.1002/polb.20967>
14. D. Cohn and A. Hotovely-Salomon, Biodegradable multiblock PEO/PLA thermoplastic elastomers: molecular design and properties, *Polymer* **46** (2005) 2068–2075; <https://doi.org/10.1016/j.polymer.2005.01.012>
15. H. W. Starkweather Jr., Clustering of water in polymers, *J. Polym. Sci. Part B Polym. Lett.* **1** (1963) 133–138; <https://doi.org/10.1002/pol.1963.110010305>
16. I. Caraballo, Factors affecting drug release from hydroxypropyl methylcellulose matrix systems in the light of classical and percolation theories, *Expert Opin. Drug Deliv.* **7** (2010) 1291–1301; <https://doi.org/10.1517/17425247.2010.528199>
17. J. D. Bonny and H. Leuenberger, Matrix type controlled release systems: I. Effect of percolation on drug dissolution kinetics, *Pharm. Acta Helv.* **66** (1991) 160–164.
18. A. Aharony and D. Stauffer, *Introduction to Percolation Theory*, Revised ed, Taylor & Francis, London, 2003.
19. T. Gonçalves-Araújo, A. R. Rajabi-Siahboomi and I. Caraballo, Application of percolation theory in the study of an extended release verapamil hydrochloride formulation, *Int. J. Pharm.* **361** (2008) 112–117; <https://doi.org/10.1016/j.ijpharm.2008.05.022>
20. I. Fuertes, A. Miranda, M. Millán and I. Caraballo, Estimation of the percolation thresholds in acyclovir hydrophilic matrix tablets, *Eur. J. Pharm. Biopharm.* **64** (2006) 336–342; <https://doi.org/10.1016/j.ejpb.2006.05.009>

21. S. Baumgartner, G. Lahajnar, A. Sepe and J. Kristl, Quantitative evaluation of polymer concentration profile during swelling of hydrophilic matrix tablets using  $^1\text{H}$  {NMR} and {MRI} methods, *Eur. J. Pharm. Biopharm.* **59** (2005) 299–306; <http://doi.org/10.1016/j.ejpb.2004.08.010>
22. Y. Y. Chen, L. P. Hughes, L. F. Gladden and M. D. Mantle, Quantitative ultra-fast MRI of HPMC swelling and dissolution, *J. Pharm. Sci.* **99** (2010) 3462–3472; <https://doi.org/10.1002/jps.22110>
23. P. P. Dorożyński, P. Kulinowski, A. Mlynarczyk and G. J. Stanisz, MRI as a tool for evaluation of oral controlled release dosage forms, *Drug Discov. Today* **17** (2012) 110–123; <https://doi.org/10.1016/j.drudis.2011.10.026>
24. U. Mikac, J. Kristl and S. Baumgartner, Using quantitative magnetic resonance methods to understand better the gel-layer formation on polymer-matrix tablets, *Expert Opin. Drug Deliv.* **8** (2011) 677–692; <https://doi.org/10.1517/17425247.2011.566554>
25. A. Hu, C. Chen, M. D. Mantle, B. Wolf, L. F. Gladden, A. Rajabi-Siahboomi, S. Missaghi, L. Mason and C. D. Melia, The properties of HPMC:PEO extended release hydrophilic matrices and their response to ionic environments, *Pharm. Res.* **34** (2017) 941–956; <https://doi.org/10.1007/s11095-016-2031-0>
26. T. M. Hyde and L. F. Gladden, Simultaneous measurement of water and polymer concentration profiles during swelling of poly(ethylene oxide) using magnetic resonance imaging, *Polymer* **39** (1998) 811–819; [http://doi.org/10.1016/S0032-3861\(97\)00328-5](http://doi.org/10.1016/S0032-3861(97)00328-5)
27. T. Tajiri, S. Morita, R. Sakamoto, M. Suzuki, S. Yamanashi, Y. Ozaki and S. Kitamura, Release mechanisms of acetaminophen from polyethylene oxide/polyethylene glycol matrix tablets utilizing magnetic resonance imaging, *Int. J. Pharm.* **395** (2010) 147–153; <https://doi.org/10.1016/j.ijpharm.2010.05.021>
28. S. Abrahmsén-Alami, A. Körner, I. Nilsson and A. Larsson, New release cell for {NMR} microimaging of tablets: swelling and erosion of poly(ethylene oxide), *J. Pharm. Biomed. Anal.* **342** (2007) 105–114; <http://doi.org/10.1016/j.ijpharm.2007.05.005>
29. Q. Zhang, L. Gladden, P. Avalle and M. Mantle, In vitro quantitative  $^1\text{H}$  and  $^{19}\text{F}$  nuclear magnetic resonance spectroscopy and imaging studies of fluvastatin<sup>TM</sup> in Lescol<sup>®</sup> XL tablets in a USP-IV dissolution cell, *J. Control. Release* **156** (2011) 345–354; <https://doi.org/10.1016/j.jconrel.2011.08.039>
30. C. Dahlberg, S. V. Dvinskikh, M. Schuleit and I. Furó, Polymer swelling, drug mobilization and drug recrystallization in hydrating solid dispersion tablets studied by multinuclear NMR micro-imaging and spectroscopy, *Mol. Pharm.* **8** (2011) 1247–1256; <https://doi.org/10.1021/mp200051e>
31. C. A. Fyfe and A. I. Blazek, Investigation of hydrogel formation from hydroxypropylmethylcellulose (HPMC) by NMR spectroscopy and NMR imaging techniques, *Macromolecules* **30** (1997) 6230–6237; <https://doi.org/10.1021/ma970076o>
32. C. A. Fyfe, H. Grondey, A. I. Blazek-Welsh, S. K. Chopra and B. J. Fahie, {NMR} imaging investigations of drug delivery devices using a flow-through {USP} dissolution apparatus, *J. Control. Release* **68** (2000) 73–83; [http://doi.org/10.1016/S0168-3659\(00\)00237-6](http://doi.org/10.1016/S0168-3659(00)00237-6)
33. L. Maggi, L. Segale, M. L. Torre, E. Ochoa Machiste and U. Conte, Dissolution behaviour of hydrophilic matrix tablets containing two different polyethylene oxides (PEOs) for the controlled release of a water-soluble drug. Dimensionality study, *Biomaterials* **23** (2002) 1113–1119; [https://doi.org/10.1016/S0142-9612\(01\)00223-X](https://doi.org/10.1016/S0142-9612(01)00223-X)
34. H. D. Bale and P. W. Schmidt, Small-angle X-ray-scattering investigation of submicroscopic porosity with fractal properties, *Phys. Rev. Lett.* **53** (1984) 596–599; <https://doi.org/10.1103/PhysRevLett.53.596>
35. S. Baumgartner, G. Lahajnar, A. Sepe and J. Kristl, Investigation of the state and dynamics of water in hydrogels of cellulose ethers by  $^1\text{H}$  NMR spectroscopy, *AAPS PharmSciTech* **3** (2002) 86; <https://doi.org/10.1208/pt030436>

36. B. Narasimhan and N. A. Peppas, Molecular analysis of drug delivery systems controlled by dissolution of the polymer carrier, *J. Pharm. Sci.* **86** (1997) 297–304; <https://doi.org/10.1021/jsp960372z>
37. N. A. Peppas and J. J. Sahlin, A simple equation for the description of solute release. III. Coupling of diffusion and relaxation, *Int. J. Pharm.* **57** (1989) 169–172; [https://doi.org/10.1016/0378-5173\(89\)90306-2](https://doi.org/10.1016/0378-5173(89)90306-2)
38. T. Higuchi, Mechanism of sustained-action medication. Theoretical analysis of rate of release of solid drugs dispersed in solid matrices, *J. Pharm. Sci.* **52** (1963) 1145–1149; <https://doi.org/10.1002/jps.2600521210>
39. R. W. Korsmeyer, R. Gurny, E. Doelker, P. Buri and N. A. Peppas, Mechanisms of solute release from porous hydrophilic polymers, *Int. J. Pharm.* **15** (1983) 25–35; [https://doi.org/10.1016/0378-5173\(83\)90064-9](https://doi.org/10.1016/0378-5173(83)90064-9)
40. A. Körner, A. Larsson, A. Andersson and L. Piculell, Swelling and polymer erosion for poly(ethylene oxide) tablets of different molecular weights polydispersities, *J. Pharm. Sci.* **99** (2010) 1225–1238; <https://doi.org/10.1002/jps.21892>
41. M. Efentakis and M. Vlachou, Evaluation of high molecular weight poly(oxyethylene) (Polyox) polymer: studies of flow properties and release rates of furosemide and captopril from controlled-release hard gelatin capsules, *Pharm. Dev. Technol.* **5** (2000) 339–46; <https://doi.org/10.1081/PDT-100100549>
42. H. Li, R. J. Hardy and X. Gu, Effect of drug solubility on polymer hydration and drug dissolution from polyethylene oxide (PEO) matrix tablets, *AAPS PharmSciTech* **9** (2008) 437–443; <https://doi.org/10.1208/s12249-008-9060-x>
43. L. Wang, K. Chen, H. Wen, D. Ouyang, X. Li, Y. Gao, W. Pan and X. Yang, Design and evaluation of hydrophilic matrix system containing polyethylene oxides for the zero-order controlled delivery of water-insoluble drugs, *AAPS PharmSciTech* **18** (2017) 82–92; <https://doi.org/10.1208/s12249-016-0498-y>
44. C.-J. Kim, Effects of drug solubility, drug loading, and polymer molecular weight on drug release from Polyox tablets, *Drug Dev. Ind. Pharm.* **24** (1998) 645–651; <https://doi.org/10.3109/03639049809082366>
45. D. H. Choi, J. Y. Lim, S. Shin, W. J. Choi, S. H. Jeong and S. Lee, A novel experimental design method to optimize hydrophilic matrix formulations with drug release profiles and mechanical properties, *J. Pharm. Sci.* **103** (2014) 3083–3094; <https://doi.org/10.1002/jps.24080>
46. J. S. Park, J. Y. Shim, K. V. T. Nguyen, J. S. Park, S. Shin, Y. W. Choi, J. Lee, J.-H. Yoon and S. H. Jeong, A pharma-robust design method to investigate the effect of PEG and PEO on matrix tablets, *Int. J. Pharm.* **393** (2010) 79–87; <https://doi.org/10.1016/j.ijpharm.2010.04.009>
47. P. Draksler, B. Janković, Z. Abramović, Z. Lavrić and A. Meden, Assessment of critical material attributes of polyethylene oxide for formulation of prolonged-release tablets, *Drug Dev. Ind. Pharm.* **45** (2019) 1949–1958; <https://doi.org/10.1080/03639045.2019.1689991>
48. A. P. Cruz, C. D. Bertol, H. K. Stulzer, F. S. Murakami, F. T. Costella, H. V. A. Rocha and M. A. S. Silva, Swelling, erosion, and release behavior of PEO/primaquine matrix tablets, *Pharm. Chem. J.* **42** (2008) 413–418; <https://doi.org/10.1007/s11094-008-0137-3>
49. H. Kojima, K. Yoshihara, T. Sawada, H. Kondo and K. Sako, Extended release of a large amount of highly water-soluble diltiazem hydrochloride by utilizing counter polymer in polyethylene oxides (PEO)/polyethylene glycol (PEG) matrix tablets, *Eur. J. Pharm. Biopharm.* **70** (2008) 556–562; <https://doi.org/10.1016/j.ejpb.2008.05.032>
50. Colorcon, Physico-mechanical characterization of POLYOX for tablet manufacture, 2009.
51. T. D. Reynolds, S. A. Mitchell and K. M. Balwinski, Investigation of the effect of tablet surface area/volume on drug release from hydroxypropylmethylcellulose controlled-release matrix tablets, *Drug Dev. Ind. Pharm.* **28** (2002) 457–466; <https://doi.org/10.1081/DDC-120003007>

52. S.-U. Choi, J. Lee and Y. W. Choi, Development of a directly compressible poly(ethylene oxide) matrix for the sustained-release of dihydrocodeine bitartrate, *Drug Dev. Ind. Pharm.* **29** (2003) 1045–1052; <https://doi.org/10.1081/DDC-120025863>
53. Colorcon, Formulation of Polyox ER matrices for a highly soluble active, 2009.
54. Q. Zhang, Investigating polymer conformation in poly (ethylene oxide) (PEO) based systems for pharmaceutical applications a Raman spectroscopic study of the hydration process, Department of Applied Physics, Condensed Matter Physics, Chalmers University of Technology, 2011.
55. A. Rangriz Shokri, T. Babadagli and A. Jafari, A critical analysis of the relationship between statistical- and fractal-fracture-network characteristics and effective fracture-network permeability, *SPE Reserv. Eval. Eng.* **19** (2016) 494–510; <https://doi.org/10.2118/181743-PA>
56. E.-Q. Chen, S.-W. Lee, A. Zhang, B.-S. Moon, P. S. Honigfort, I. Mann, H.-M. Lin, F. W. Harris, S. Z. D. Cheng, B. S. Hsiao and F. Yeh, Isothermal thickening and thinning processes in low molecular weight poly(ethylene oxide) fractions crystallized from the melt: 6. Configurational defects in molecules, *Polymer* **40** (1999) 4543–4551; [https://doi.org/10.1016/S0032-3861\(99\)00069-5](https://doi.org/10.1016/S0032-3861(99)00069-5)
57. The Dow Chemical Company, What is the glass transition temperature of POLYOX™ water-soluble resins?, Dow Answ. Cent.; [https://dowservice.custhelp.com/app/answers/detail/a\\_id/17872](https://dowservice.custhelp.com/app/answers/detail/a_id/17872) (accessed October 24, 2019).
58. S. Sant, V. Nadeau and P. Hildgen, Effect of porosity on the release kinetics of propafenone-loaded PEG-g-PLA nanoparticles, *J. Control. Release* **107** (2005) 203–214; <https://doi.org/10.1016/j.jconrel.2005.02.017>
59. J. Ma, J. Sun, L. Fan, S. Bai, H. Panzai and Y. Jiao, Fractal evolution of dual pH- and temperature-responsive P(NIPAM-co-AA)@BMMs with bimodal mesoporous silica core and coated-copolymer shell during drug delivery procedure via SAXS characterization, *Arab. J. Chem.* **13** (2020) 4147–4161; <https://doi.org/10.1016/j.arabjc.2019.06.012>